Eur. Phys. J. B **13**, 387–393 (2000)

THE EUROPEAN PHYSICAL JOURNAL B

EDP Sciences

A multi-species lattice-gas automaton model to study passive and reactive tracer migration in 2D fractures

V. Pot[a] and T. Karapiperis[b]

Paul Scherrer Institute, Würenlingen and Villigen, 5232 Villigen PSI, Switzerland

Received 14 January 1999 and Received in final form 8 June 1999

Abstract. We developed a numerical model based on a multi-species lattice gas cellular automaton to study passive and reactive tracer migration in saturated geological media. The model was made of multiple lattice gases interacting *via* a two-species collision rule. For a binary mixture, the model displayed a negative deviation from Raoult's law and therefore behaved as a real solution. By biasing the initial two-species collision rule, our model was made to obey the tracer assumption which requires that the tracer species does not affect the velocity of the vehicle fluid. In a 2D fracture, we checked the Taylor-Aris relation. An irreversible adsorption between the tracer and the solid phase was numerically added to perform filtration of the colloids. A good agreement was found with the solution of the filtration equation. An attachment efficiency was defined and was found to bear a linear relationship to the filtration coefficient. We added a third species to study the potential role of colloids in the transport of contaminants. Contaminant migration was enhanced when contaminants were bound to colloids and was slightly reduced when colloids were allowed to adsorb on the solid phase.

PACS. 47.55.Kf Multiphase and particle-laden flows – 82.70.Dd Colloids – 47.55.Mh Flow through porous media

1 Introduction

In the framework of the assessment of nuclear repositories safety the migration of radioactive pollutants in fractured geological media has been widely investigated. Transport models traditionally partitioned radionuclides between a mobile and an immobile phase. It was established that, because of diffusion into the rock matrix adjacent to the fractures and adsorption on the matrix pore walls, the radionuclides, released from the repository, were delayed in their migration through the fractures of the host rock. However, within the past two decades experimental data provided evidence for a third phase in the contaminant migration process: the potential role for colloid-bound radionuclides [1–3]. Transport of contaminants can be either enhanced or diminished by the presence of colloids (*e.g.* [4–6]). Therefore, a model that would predict radionuclide pollution in fractured geological media must account accurately for colloid material transport.

The objective of this paper is mainly methodological. We present a new multi-species lattice gas automaton (LGA) model developed in order to study the colloid filtration in saturated geological media and the potential role of colloids in the transport of contaminants. The model is based on the concept of multiple LGA interacting through microscopic diffusion rules. Lattice gases are a class of cellular automata appropriate for describing fluid dynamics. Briefly stated, these models simulate a discretized fluid in velocity, space and time (full description can be found in [7]).

The principle of the multi-species LG model and its physical and hydrodynamical properties are described in Section 2. Then, we apply the model to the dispersion of a passive tracer through a 2D fracture. Finally the filtration of a reactive tracer and the transport of a contaminant species bound to either a passive or a reactive tracer are described in Section 4.

2 The multi-species model

2.1 Principle

LG and LB models have already been extended to multi-species models to study the behavior of a passive scalar [8–10] and, recently, of a reactive tracer [11]. Unlike the LG models, the LB models do not exhibit statistical noise and a large range of viscosities and molecular diffusion coefficients can be used [12]. In the case of

[a] *Present address*: Laboratoire de Biogéochimie Isotopique, Université P. et M. Curie, UMR 7618 CNRS-Université P. & M. Curie-INRA, Tour 26, case 120, 4 place Jussieu, 75252 Paris Cedex 05, France
e-mail: `pot@ccr.jussieu.fr`

[b] *Present address*: European Parliament, Rue Belliard 97-113, 1047 Bruxelles, Belgium

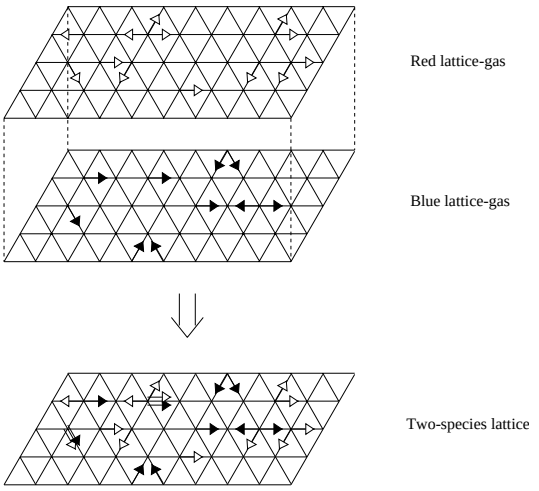

Fig. 1. The principle of the construction of the multi-species lattice is to sum multiple parallel overlying one-species lattice. The model is presented here with two species. The white arrows represent the red particles and the black arrows represent the blue particles. The cells of the two-species lattice can be occupied by at most two particles, one of red type and one of blue type. At each time step, each type of particles hop from one site to another site according to their velocity vector and undergo the one-species collisions of the FHP-I model on their own colored lattice. Then, the red and blue particles interact with each other by means of a two-species collision rule defined in the next figure.

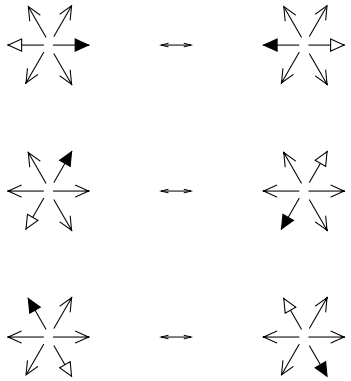

Fig. 2. Reversible two-species collision rule. Red and blue particles are labeled with white closed arrows and black closed arrows respectively. Open arrows represent any occupation by any color of particles. A maximal momentum of -4 is exchanged at a site for each collision. Although the collisions did not conserve the color-momentum, they conserved the total momentum.

the LG models, viscosity and molecular diffusion coefficient are generated by the microscopic rules. They are density-dependent and are not allowed to be easily independently varied. However, we chose the boolean LG approach because it allowed us: i) to introduce, with the help of simple microscopic rules, a set of elementary adsorption processes, and ii) to study the effect of different hydrodynamical conditions (various velocities, different size of fractures) on the filtration of colloids and the transport of contaminants. In fact, the multiple LG approach allowed us to follow the exact hydrodynamics of each species and consider various adsorption processes (solid-colloid, contaminant-colloid).

We built our multi-species LG model as the summation of the configurations of multiple overlying parallel lattices, each containing an ensemble of the same color of particles moving on their assigned lattice, according to the rules of the FHP-I model[1] (Fig. 1). At each node, particles of different type interacted together according to a two-species collision rule that was chosen to minimize the molecular diffusion coefficient (Fig. 2) and so increase diffusion times compared to hydrodynamic times. These rules depended on the local position of the different colored particles. They could be compared to Rothman and Keller' diffusion rules that depend on the local color gradient and create, in their case, surface tension effects [15]. The exclusion principle did not hold anymore on the multi-species lattice although it held on each colored lattice. This approach overcame the main limitation of other multi-species LG models [8]: it allowed us to add as many different species as one needs without including an increase in the statistical noise of calculations since, for each species, the range of particle density was the same as for the mono-species model.

For our purpose, up to three species were studied: the vehicle species (blue particles), the colloid species (red particles) and the contaminant species (green particles). In the following section, we study the physical properties of our multi-species model restricted to two species.

2.2 State equation and Raoult's law

An interesting property of our multi-species LG model was that the equilibrium partial pressures could be simply calculated for each component. The total pressure of a binary mixture, containing red and blue particles, was defined as the sum of the red and blue pressures. For a homogeneous distribution of red and blue particles, it is given by:

$$p = p_{\mathrm{r}} + p_{\mathrm{b}} = 3d + 3\gamma\theta_{\mathrm{r}}d(1-\theta_{\mathrm{r}}d)(1-\theta_{\mathrm{r}})d(1-(1-\theta_{\mathrm{r}})d) \quad (1)$$

with $d = d_{\mathrm{r}} + d_{\mathrm{b}}$ the total (red plus blue) reduced density, $\gamma = -4$ the total momentum transferred in a two-species collision and $\theta_{\mathrm{r}} = d_{\mathrm{r}}/d$ the relative red concentration. The first term of the last expression in (1) corresponds to the momentum flux due to the propagation of red and blue particles and the second term, calculated according [16]

[1] We chose the FHP-I version (among the FHP models [7]) because the filtration of colloids in geological media involves small natural velocities, usually of a few meters per year [13]. The experimental Darcy's law that holds in these situations is valid for a Reynolds number lower than about 10. The FHP-I model corresponds to a comparable value and obeys Darcy's law [14].

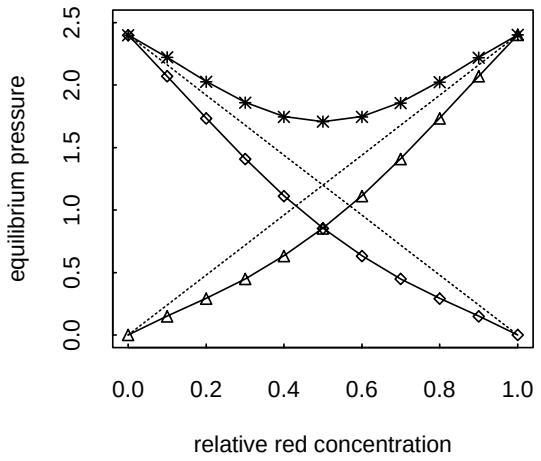

Fig. 3. Equilibrium pressures measured for different relative red concentrations at fixed total reduced density ($d = 0.8$ particle per cell). Symbols represent the results of numerical simulations. Triangles, diamonds and stars are the measured red, blue and total pressures, respectively. Solid lines are the corresponding theoretical pressures calculated as described in the text. We drew Raoult's law prediction for each component with dotted lines. The units of the pressure are [mass units/(lattice units × time unit squared)].

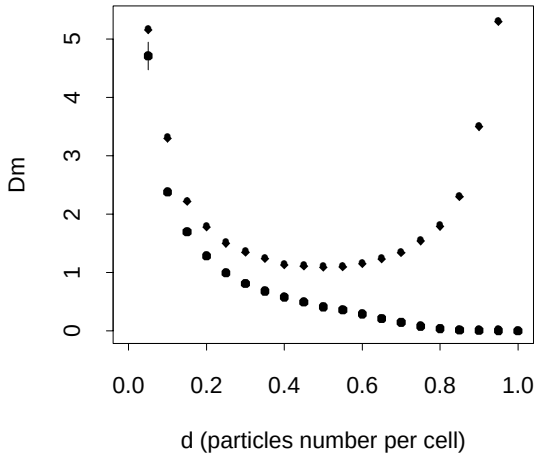

Fig. 4. Measured molecular diffusion coefficients *versus* reduced density. Squared symbols are the D_{m} values measured with the two-species collision rules of Figure 2, and diamonds are the D_{m} values measured with the biased two-species collision rules of Figure 5. The units of the diffusion coefficient are $[lu^2/tu]$.

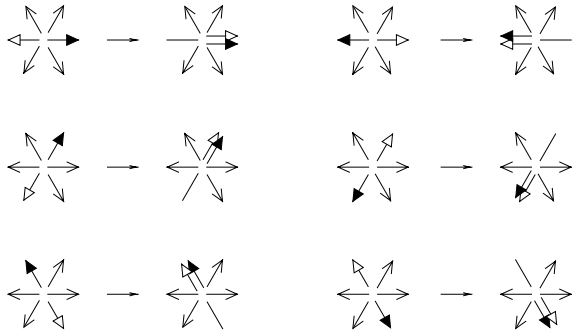

Fig. 5. Biased two-species collision rule. Legend is the same as Figure 2 with no arrows representing no particles. A maximal momentum of -2 is exchanged at a site for each collision.

corresponds to the momentum flux due to the collision between red and blue particles.

We randomly distributed a uniform density of red and blue particles in boxes containing 64×64 nodes and let the system evolve for 2000 time units (tu). To measure the partial pressure of each component, we defined links rather than nodes as counters of the exchanged momentum. A positive contribution of $+1$ was given for propagating particles and a negative contribution of -2 was given for colliding particles. Results are plotted in Figure 3. The numerical measurements of red and blue pressures displayed perfect agreement with the theoretical pressure previously calculated (Eq. (1)). We observed negative deviations from ideal solution behavior [17], although the partial pressure of the components at the highest and lowest concentrations approached the values given by Raoult's law. We concluded that our model behaved as a real solution where the interaction between the two species was stronger than the interaction between particles of same color.

2.3 Molecular diffusion coefficient

We checked the diffusive behavior of our model and measured the molecular diffusion coefficient by studying the time relaxation of a one-dimensional concentration step [18]. Numerical simulations were performed in boxes of size $L \times W = 320 \times 126$ nodes. A very good agreement was found between the measured data and the solution of the diffusion equation, although for reduced densities superior to 0.7 particle per cell the agreement was less satisfactory. Figure 4 displays the molecular diffusion coefficient, D_{m}, as a function of the total reduced density, d. We observed that D_{m} goes to zero as d approaches unity, since, in this particular case, our two-species collision rule prevents particles from diffusing.

3 Study of a passive tracer

3.1 A biased multi-species model

In real life, when colloids are advected by the flow, they do not perturb the velocity of the fluid [19]. In our approach, because of the coexistence of collisions between particles of same type and collisions between particles of different types, the addition of a pulse of red particles introduced density perturbations in the blue fluid, their strength being proportional to the red particle density. Statistical noise inherent in LG models required us to use non-infinitesimal tracer density. Therefore, we modified the two-species collision rule and proposed to cancel the scattering of the blue particles by the red particles. The new biased two-species collision rule is displayed in Figure 5. This was a notable change since the output

configurations did not conserve the total momentum. However, most of the features of the previous model were recovered since red diffusion occurred only if the same input configurations of the two-species collision rule described previously were met. The immediate result of this new procedure was that the blue velocity distribution was transmitted to the red particles through the biased two-species collision rule. The blue fluid therefore played the role of a body force acting on the other species.

We measured the molecular diffusion coefficient resulting from this new two-species collision rule by repeating our previous simulation of time relaxation of a one-dimensional red concentration step. Results are plotted in Figure 4. D_{m} values showed a duality against the density: for $d = 0$ and for $d = 1$, D_{m} was infinite because no red diffusion was performed. The D_{m} values obtained with the two variants of the two-species collision rule were of the same order of magnitude for $d < 0.5$, as one would expect since the two rules assumed locally the same input configurations.

3.2 Dispersion of a passive tracer

We checked the dispersive behavior of the biased multi-species model by studying the time evolution of a tracer concentration continuously injected into a fluid flowing between two parallel walls [8].

Initially, the channel of size 4000×28 nodes was uniformly filled with a blue fluid of reduced density $d_{\mathrm{b}} = 0.6$ particle per cell. A constant blue flow was generated by probabilistically biasing the x-momentum of the blue particles. We used this numerical method because the stationary Poiseuille velocity distribution was obtained much faster than when applying a pressure gradient. Then, at the left boundary of the channel, we continuously injected the inert tracer of reduced density $d_{\mathrm{r}0} = 0.2$ particle per cell. The normalized red particle density, $d_{\mathrm{r}}(x,t)/d_{\mathrm{r}0}$, obtained in our simulations was in good overall agreement with the analytical solution of the standard convection-dispersion equation. We successfully checked that the mean distance $\langle x \rangle$ traveled by the tracer concentration equaled Ut with U the mean tracer velocity.

We checked, for U ranging from 0.035 to 0.315 $lu.tu^{-1}$ (Peclet number $Pe = \frac{Ua}{D_{\mathrm{m}}}$ ranging from 0.47 to 4.27), that the model obeyed Taylor's relation [20] calculated in the case of two parallel plates with aperture a [21]:

$$D_L = D_{\mathrm{m}} + \frac{U^2 a^2}{210 D_{\mathrm{m}}} \tag{2}$$

with D_L the dispersion coefficient. We found a linear relation between D_L and U^2 (Fig. 6): $D_L = (1.78 \pm 0.04) + (2.5 \pm 0.8)U^2$.

A constant coefficient of 1/210 appears in Taylor's relation (2). Taking $D_{\mathrm{m}} = 1.78 \pm 0.04$ and $a = 28\sqrt{3}/2\ lu$, we calculated a constant coefficient from the slope of our linear relation and found it to differ by a factor of 1.6 ± 0.5 from Taylor's prediction. The D_{m} value extracted from our linear relation is very close to the value obtained in Section 3.1 (1.79 ± 0.04).

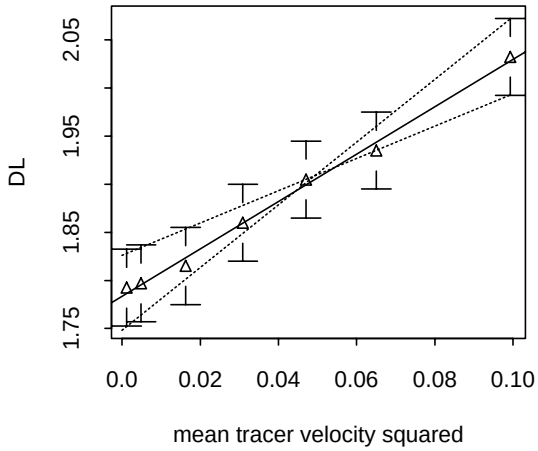

Fig. 6. Longitudinal dispersion coefficient *versus* the square of the mean tracer velocity. Symbols are the measured values and the solid line is the best least-square-fit. The dashed lines gives the uncertainty of the slope and the regress intercept. Units are $[lu^2/tu]$ for D_L and $[(lu/tu)^2]$ for the V^2.

4 Study of reactive tracer

4.1 Adsorption isotherm

We simulated the deposition of colloids on the solid phase with a very simple procedure. We defined the following irreversible adsorption: a solid site adsorbed a particle once every n collisions. Adsorbed particle were removed from the lattice. We calculated the attachment efficiency α, defined as the ratio of the number of collisions that succeed in producing adhesion to the number of collisions which occur between suspended particles and the solid phase [22], and we found $\alpha = \frac{1}{n}$. The model was able to deal with the full range of possible situations, from the no-adsorption case ($\alpha = 0$) to the infinite sink boundary condition ($\alpha = 1$).

One can calculate the theoretical adsorption isotherm. Let S_n be the number of tracer particles adsorbed per solid site and per time step. Because of the hexagonal geometry of the lattice, S_n is dependent of the geometry of the solid phase. In the case of a wall parallel to one of the three directions of the lattice, the averaged number of particles per solid site is equal to one third of the averaged number of particles per non-solid site. Therefore, and from the definition of our irreversible adsorption rule, the adsorption isotherm reads:

$$S_n = \frac{1}{3n}\rho_{\mathrm{r}}. \tag{3}$$

We numerically measured the adsorption isotherm in the case of a channel geometry of $L \times W = 256 \times 32$ nodes. The channel was initially filled with a uniform blue fluid of density ρ_{b} and a uniform red fluid of density ρ_{r}. At each time step, the density of the red fluid was kept constant by re-injecting the exact number of adsorbed red particles. An equilibrium between the number of injected red particles and the number of adsorbed red particles was rapidly reached. For these simulations, n was fixed to 30.

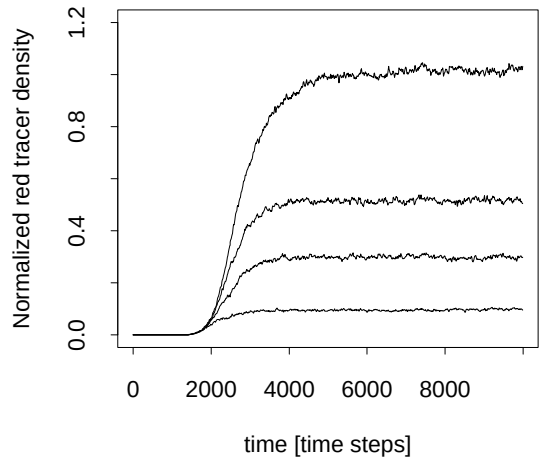

Fig. 7. Normalized red density *versus* time measured at a distance of 300 nodes from the inlet. The top curve corresponds to the non-adsorbing case, and from top to bottom the three other curves correspond to adsorbing tracer with $n = 60$, 30 and 15, respectively. Tracer was injected 1000 time steps after initial time. Each curve is the average of ten repetitions.

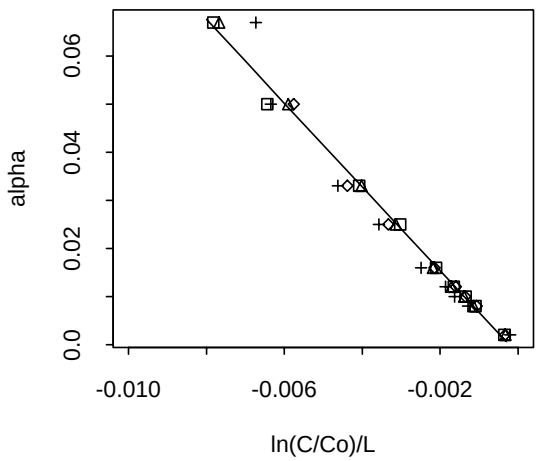

Fig. 8. Attachment efficiency coefficient, α, against $\ln(C/C_0)/L$. The measures were performed at the following fixed different distances L from the injection of the tracer: 100 lu (+), 200 lu ($\triangle$), 500 lu ($\square$) and 800 lu ($\diamond$). Solid line is the best least-square fit (see relation (5) in text).

We counted the total number N_A of red particles adsorbed onto the solid phase during $T = 2000\ lu$. Then, we calculated S_n as $N_A/(2LT)$. We repeated the simulation for different values of ρ_r and we found the following linear relation: $S_{30} = 0.011\rho_r$ which was in perfect agreement with the analytical relation (3).

4.2 Numerical experiment of filtration of a reactive tracer

We resumed the experiment of dispersion of a tracer through two parallel walls of Section 3.2 for a mean red velocity equal to 0.175 $lu.tu^{-1}$. We repeated the experiment for different values of n ranging from 15 to 500. We measured the red concentration inside the channel as a function of time at fixed distances $L = 100$, 300, 500 and 800 lu from the injection inlet. The measures were averaged over the thickness of the channel and over the range $[L-10, L+10]$. The resulting elution curves are displayed in Figure 7. The normalized red concentration, expressed as the ratio of the red concentration to the injected red concentration, was plotted against time for three different rates of adsorption: $n = 15$, 30 and 60 and at $L = 300\ lu$. After about 4000 tu a plateau was reached which meant that an equilibrium was obtained between the injected red concentration and the adsorbed one. We compared our results with the solution of the filtration equation proposed by Iwasaki (1937)[23]:

$$\frac{C}{C_0} = \exp(-\lambda L) \tag{4}$$

with λ the filtration coefficient, L the length of the filtering medium, C_0 the influent concentration of tracer and C the effluent concentration obtained after the complete breakthrough of the tracer. We found the following linear relation between α and $\ln \frac{C}{C_0}$ (Fig. 8):

$$\alpha = -(8.7 \pm 0.3)\frac{1}{L}\ln\frac{C}{C_0}\cdot \tag{5}$$

Therefore, from equations (4, 5) we established the straightforward relation between the filtration coefficient λ and our attachment efficiency α:

$$\lambda = \frac{\alpha}{8.7}\cdot \tag{6}$$

In Figure 9, the tracer concentration profiles are displayed for all L and for four different rates of adsorption ($n = 15$, 30, 60 and ∞) together with the solution of the basic filtration equation (4) using the value of λ obtained from (6). The agreement is perfect for attachment efficiencies close to one but small discrepancies are observed for weaker adsorption.

4.3 Colloid-bound contaminant migration

We used our model with three species in order to study the potential role of colloids in the contaminant migration process. Recent experimental measurements showed that radionuclides of low aqueous solubility were transported significant distance from their source than would be expected from their solubility [3]. We investigated therefore whether our model was able to account quantitatively for these effects through adsorption of the contaminant species onto the colloidal phase. To this end, we compared numerically the migration velocities of a green (contaminant) and a red (colloid) concentration pulse that were advected by a blue (vehicle) fluid in a channel of size 3000×128 sites. The colloid pulse traveled at a constant mean velocity $U_r = 0.193\ lu.tu^{-1}$, and the contaminant pulse traveled at a lower constant mean velocity $U_g = 0.16\ lu.tu^{-1}$. Different initial densities ($d_r = 0.6$ and $d_g = 0.2$ particle per

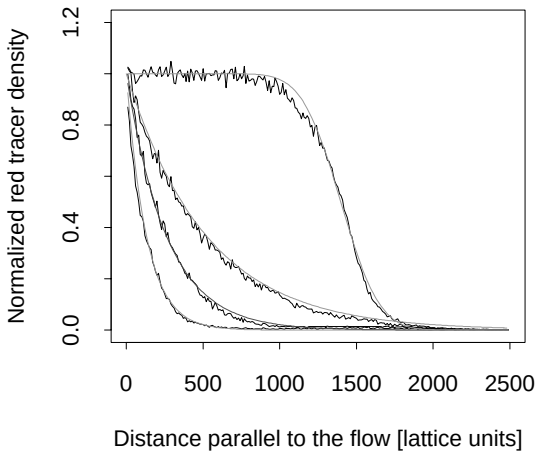

Fig. 9. Normalized red density profiles against the length of the channel. The top curve is the result of the non-adsorbing spreading tracer fitted to the advection-dispersion analytical solution. The adsorbing tracer concentration profiles displayed correspond to values of n equal to 60, 30 and 15 from top to bottom respectively.

cell) allowed us to simulate a macroscopic delay in the contaminant species migration. In real systems, such differences in velocity can arise for instance from the different solubilities of the contaminant species. In Figure 10a are displayed the mean distances $\langle x \rangle$ traveled by the pulses as a function of time.

In a first simulation, the contaminant was allowed to adsorb on the mobile colloidal phase. Once a green particle was adsorbed on a red particle, it followed the exact dynamics of the red particle. No more than one green particle could be adsorbed onto a red particle. In this situation, adsorption took place each time a free red particle encountered a green particle on the same cell. The resulting velocity of the colloid-bound contaminant was found to be the same as that of the colloid (0.194 $lu.tu^{-1}$). This result was expected, since within 100 tu the whole ensemble of green particles was adsorbed onto the red particles. We repeated the simulation with a fixed constant probability $\beta = 0.002$ for the green particles to get adsorbed. The resulting migration velocity, $U_g = 0.188\ lu.tu^{-1}$, is intermediate between that of the free contaminant and that of the totally colloid-bound contaminant (Fig. 10a). After 5000 tu, about 80 % of the total green particles got adsorbed onto colloidal particles.

In a second simulation, we studied the role played by the filtration of the colloidal phase in the migration of the colloid-bound contaminant. The simulation was performed with the filtration of the colloids described by an attachment efficiency $\alpha = 0.066$ and with the probability $\beta = 0.002$ for green particles to get adsorbed on the colloids. The resulting migration mean distances are displayed in Figure 10b. A linear variation with time was found after 2000 tu for the colloidal pulse and for the colloid-bound contaminant pulse. Calculated velocities were found to be 0.169 $lu.tu^{-1}$ and 0.137 $lu.tu^{-1}$, respectively. The latter velocity was inferior to that of free contaminant migration. We showed that the colloidal phase can have a disastrous effect on the migration of contaminants, since, in the absence of colloid filtration, the velocity of green particles was significantly enhanced (by a factor of about 1.2). However, filtration of colloids has a beneficial effect since the velocity of the contaminant was significantly reduced in our simulations.

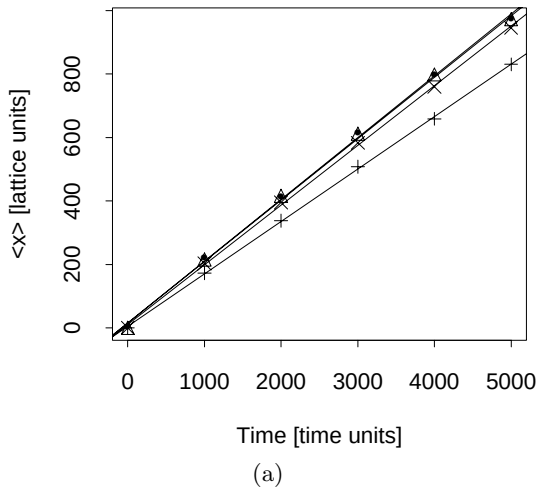

(a)

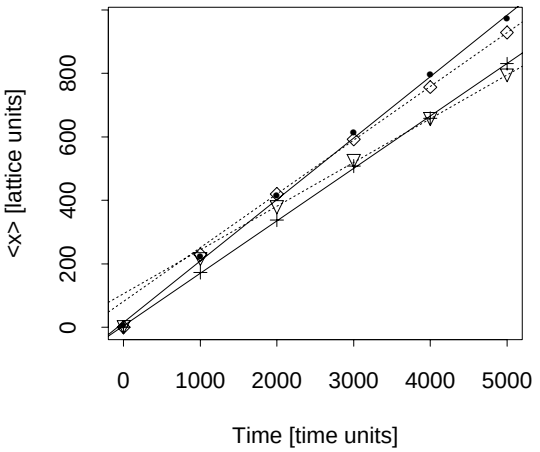

(b)

Fig. 10. (a) Mean distances traveled by the following different concentration steps against time: colloids (•), free contaminants (+), contaminants entirely bound to colloids (△) and contaminants partly bound to colloids (×) are displayed. Solid lines are the best least-square fits. (b) Mean distances traveled by the following different concentration steps against time: colloids undergoing an adsorption onto the solid phase (◇) and contaminants partly bound to this colloidal phase. (▽) Dashed lines are the best least-square fits calculated after 2000 tu. Results obtained for colloids and contaminants in the cases with no adsorption (colloid-contaminants and colloid-solid phase) are also displayed. Their legend is the same as in (a).

5 Conclusions

We constructed a multi-species LG model from multiple reacting lattice gases. This new approach allowed us to calculate the partial pressure of each component of a binary mixture. We modified the microscopic diffusion rules of our model in order to study tracer filtration and contaminant migration velocities. In our simulations, we obtained a constant velocity of the mean displacement of the tracer concentration as expected.

The objective of this paper was mainly methodological. We showed that we could easily implement different processes such as colloid-contaminant and solid-colloid adsorption and combine them in a simple way. We concluded from these simulations that, when using simple irreversible adsorption procedures onto mobile and immobile phases, the model was able to describe quantitatively the influence of the colloidal phase, as well as of colloid filtration on contaminant migration. Our results show that colloid filtration plays a crucial role in contaminant migration. Therefore the concept of interacting multiple LG models can constitute a useful basis for further investigations in the migration of contaminants.

A specific question one can address on the basis of our results concerns the meaning of the coefficient of proportionality found between the filtration coefficient and the attachment efficiency. For instance, filtration performed with different velocities should establish whether the model incorporates hydrodynamical effects in the filtration mechanism. In this paper, only irreversible adsorption procedures were implemented. Interesting extensions of this work would involve introducing more complex microscopic rules in order to model at a more elementary level the interactions between mobile and immobile phases. Thus, to incorporate adsorption kinetics, a desorption procedure should be added so that the sorption processes become dependent on the local concentration of the relevant type of particles, following the Immiscible Lattice Gas approach [15]. The parameters α and β (colloid attachment efficiency on the solid phase and probability for adsorption of a contaminant particle on a colloidal particle) obtained from the LG simulation can serve as phenomenological predictions for analogous parameters derived from microscopic models based on the fundamental electrostatic interactions between the actual particles. Such attractive forces can also be modeled using the LG approach, as it has already been done in [24] for porous media.

Valérie Pot would like to thank the modeling section (PSI) for allowing her to perform this work and especially Dr. J. Haderman and Dr. A. Jakob for fruitful discussions. She also gratefully acknowledges Prof. S. Zaleski (Université P. et M. Curie), Dr. A. Genty (CEA) and Dr. C. Appert (ENS). She thanks Prof. A. Mariotti (Université P. et M. Curie) for allowing her to complete the writing of this paper in his laboratory.

References

1. J.C. Sheppard, M.J. Campbell, T. Cheng, J.A. Kittrick, Environ. Sci. Technol. **14**, 1349 (1980).
2. R.W. Buddemeier, J.R. Hunt, Appl. Geochem. **3**, 535 (1988).
3. A.B. Kersting, D.W. Efurd, D.L. Finnegan, D.J. Rokop, D.K. Smith, J.L. Thompson, Nature **397**, 56 (1999).
4. P. Grindrod, J. Contam. Hydrol. **13**, 167 (1993).
5. P.A. Smith, C. Degueldre, J. Contam. Hydrol. **13**, 143 (1993).
6. M. Ibaraki, E.A. Sudicky, Water Resour. Res. **31**, 2945 (1995).
7. U. Frisch, D. d'Humières, B. Hasslacher, P. Lallemand, Y. Pomeau, J.-P. Rivet, Complex Systems **1**, 649 (1987).
8. C. Baudet, J.-P. Hulin, P. Lallemand, D. d'Humières, Phys. Fluids A **1**, 507 (1989).
9. H. Chen, W.H. Matthaeus, Phys. Fluids **30**, 1235 (1987).
10. X. Shan, G. Doolen, Phys. Rev. E **54**, 3614 (1996).
11. H.W. Stockman, Water Resour. Res. **33**, 1823 (1997).
12. N. Rakotomalala, D. Salin, P. Watzky, J. Fluid Mech. **338**, 277 (1997).
13. P.A. Smith, PSI Bericht Nr. 93-04, Villigen, 1993.
14. D.H. Rothman, Geophysics **53**, 509 (1988).
15. D.H. Rothman, J. Keller, J. Stat. Phys. **52**, 1119 (1988).
16. O. Tribel, J.-P. Boon, J. Stat. Phys. **81**, 361 (1995).
17. F. Daniels, R.A. Alberty, *Physical Chemistry* (John Wiley and Sons, Inc., New-York, London-Sydney, 1966).
18. D. d'Humières, P. Lallemand, J.-P. Boon, D. Dab, A. Noullez, in *Chaos and Complexity*, edited by R. Livi, S. Ruffo, S. Ciliberto, M. Buiatti (World Scientific, Singapore, 1987), pp. 278-301.
19. G. Matheron, G. de Marsily, Water Resour. Res. **16**, 901 (1980).
20. G. Taylor, Proc. Roy. Soc. A **219**, 186 (1953).
21. M.J.E. Golay, *Proceedings of Gas Chromatography held in Amsterdam* (1958), pp. 36–53.
22. K.M. Yao, M.T. Habibian, C.R. O'Melia, Environ. Sci. Technol. **5**, 1105 (1971).
23. T. Iwasaki, J. Am. Water Works Assoc. **29**, 1591 (1937).
24. V. Pot, C. Appert, A. Melayah, D.H. Rothman, S. Zaleski, J. Phys. II France **6**, 1517 (1996).